

Effect of CNC End Milling Parameters on Cu–Al–Mn Ternary Shape Memory Alloys Using Taguchi Method

N. Praveen¹ · U. S. Mallik¹ · A. G. Shivasiddaramaiah¹ ·
N. Nagabhushana² · C. Durga Prasad³  ·
Shanthala Kollur³

Received: 25 September 2023 / Accepted: 30 October 2023
© The Institution of Engineers (India) 2023

Abstract CNC milling is a common technique for material removal that is used to create components with complex shapes and features. The purpose of the experiment is to determine how the CNC milling variables would affect the milling of Cu–Al–Mn (CAM) shape memory alloys (SMAs). For the investigation, an orthogonal array (OA) of the Taguchi's L9 was employed. The CNC milling process's depth of cut, feed rate, and spindle speed were chosen as the milling machining factors to study how they affected the MRR and SR of the workpiece. The examined end outcomes identified the milling settings that were most effective. ANOVA revealed that, in comparison with other components, the feed rate had the greatest influence on surface finish. By choosing the machining settings as given by the S–N Ratio graph, the ideal value of MRR and SR with a superior surface polish may be produced. SEM was used to examine the surface texture of the Cu–Al–Mn (CAM) SMAs' milled profile.

Keywords Cu–Al–Mn SMAs · CNC end milling · Material removal rate · Surface roughness · ANOVA

Introduction

CAM SMAs have superior strength, extremely high damping, and shape memory effects when compared to conventional metals or alloys. Since these CAM SMAs can be easily produced compared to Ni–Ti SMAs, they do not require performing a vacuum casting process. Due to their lower melting temperatures, the Mn-rich CAM SMAs also have greater castability [1].

CNC machining has become increasingly indispensable in the last few decades by providing improved reliability, accuracy, and productivity. Furthermore, when compared to a traditional milling process, CNC milling offers greater ease in selecting the levels of the cutting parameters [2, 3]. Various milling methods, including side milling, end milling, plain milling, and gang milling, are used in industries. Due to its high precision, accuracy, and durability, the CNC end milling technology has gained the lead among these in the automotive, aerospace, and metal processing sectors [4]. One of the adaptable procedures that has already achieved success in the industrial sector by fulfilling needs is end milling. Any machining operation involves a number of variables that control the process. These variables are separated into ones that can be controlled and those that cannot. Rake angle, spindle rotation, feed rate, cutting speed, and depth of cut are all variables that may be changed to suit the needs. Non-controllable factors are ones that can be governed indirectly by controllable parameters rather than being directly controlled. Chip development during vibrations can happen for a variety of reasons, such as tool wear and surface roughness [5–7]. Modern CNC vertical milling technology has advanced greatly to satisfy the norms of numerous manufacturing sectors, particularly the precision metal cutting industry [8]. A multi-point cutting instrument called a cutter is one of the processes used in milling to create smooth,

✉ C. Durga Prasad
durgapras71@gmail.com

¹ Department of Mechanical Engineering, Siddaganga Institute of Technology, Tumkur, Karnataka 572103, India

² Department of Mechanical Engineering, New Horizon College of Engineering, Bengaluru, Karnataka 560103, India

³ Department of Mechanical Engineering, RV Institute of Technology and Management, Bengaluru, Karnataka 560076, India

curved, and helical surfaces. In the milling process, a work item with several cutting edges is fed through a rotating cylindrical tool. The tool's rotational axis is perpendicular to the feed vein. Surface finishing is a crucial component of any machining process in the creation of a high quality product. [9–11]. The milling technique is frequently employed in modern manufacturing due to its adaptability and precision [12, 13]. Taguchi design, which can quickly and precisely determine the appropriate surface roughness for controlling particular end milling processes [14–16].

For cutting samples to required sizes and shapes along with better surface quality and increased productivity in not much time and money. The most popular application for CNC milling is in manufacturing industries and machine shops, etc. In many machining procedures, high quality and productivity are two crucial yet crucial factors. End milling, which is conducted with the aid of a computer numerically controlled machine, is a popular technique for removing material that is used in the process of producing components with complex geometries and profiles. One component that contributes to chip formation during vibrations is tool wear, and two other factors include surface texture [17–20]. In the process of removing metal, CNC milling may create components with curved or flat shapes. The milling process may be greatly improved by improving the surface quality [21, 22]. Malay et al. [3] examined on optimization of input factors under CNC milling process on aluminium 6351. According to the results of the ANOVA, the spindle has a considerable impact on Ra, followed by the feed rate and the depth of cut. The surface finish can be improved by optimising these parameters [3]. Sahare et al. [6] conducted an evaluation of the Al2024 end milling operation. End milling's primary output machining characteristics were thought to be Ra, cutting forces, and MRR. The surface roughness, cutting pressures, and metal removal rate are all influenced by the depth of cut, cutting speed, and feed rate, according to the S/N ratio response chart. From ANOVA, cutting depth has major influence on surface roughness than cutting speed. The predicted model's predictions and the data from the experiment agreed well [6]. End milling of Inconel 7018 super alloys has been studied by Reddy Sreenivasulu et al. [7]. Taguchi's DOE provided confirmation of the Inconel 718 super alloy's machining capacity. S/N ratios and ANOVA results revealed that the feed rate and combination rotational speed had the greatest impact on burr height [7]. For aluminium alloy AA6063, Maiyar et al. [10] reported on an examination of the CNC milling parameters. The analysis revealed that Ra is mostly impacted by feed rate. With an increase in feed rate, Ra's value rose. An increase in cut depth allowed for the achievement of the maximum MRR. The process parameters used determine the type of chip that is produced. On the machining time in this case, the spindle speed was determined to be inconsequential [10].

The length, width, and thickness of chips can change when feed rates and materials are changed during milling, according to a 2017 study by L Prasetyo et al. Measurements of the chip's length, breadth, and thickness were used to ascertain its properties. The AISI 1020's hardness is what causes a chip to develop in a discontinuous pattern. The length, breadth, and thickness of the chip will all grow when the feed rate is increased, regardless of the type of material being cut. The key conclusion of this study was that it is possible to determine the degree of hardness that various kinds of materials possess by looking at the amount of chips that are produced [11]. The effect of CNC milling process parameters on Ra using aluminium alloy 7024 was reported by Routara et al. in [12]. According to the experimental findings, Ra was most significantly influenced by the tool's diameter, followed by cutting speed, depth of cut, and feed rate. Less surface roughness will be produced with a bigger tool diameter. Raising spindle speed will result in a reduction in surface roughness [12]. Raja and Baskar [13] Investigation of effect of input factors such as feed rate, speed, and depth of cut on Ra and MRR of the machined parts during milling of aluminium alloy 6065-T6 under a CNC vertical milling machine. A carbide tool cutter is used as a tool during the process. Based on Taguchi's L16 OA, experiments were performed. The main factor affecting the output is the feed rate from the ANOVA method [13].

Syeddu and colleagues [14] When CNC end milling the alloy Al6061-T6, Taguchi's method was utilised to forecast how different machining parameters will affect surface roughness. To mill the work material, uncoated and TiAlN coated carbide tools were employed. Tests comparing the two types of tools were carried out to establish which type gave a higher surface quality. According to an ANOVA, spindle speed is more important than cut depth for uncoated carbide tools. Variations in cut depth and spindle speed affect the quality of the surface roughness. The main factor affecting coated tools is also spindle speed rather than feed rate. Cut depth has little to no effect on surface finish. 2500 rpm, 150 mm/min, and 0.6 mm were found to be the ideal parameter values for the sample that was machined using a carbide tool coated in TiAlN. For the coated carbide tool, a surface roughness of 0.1406 mm is ideal [14]. George et al. [15] investigated on AISI 410 and AISI 420 Martensitic Stainless Steel (MSS) dry milling characteristics and were optimised. Optimal machining parameters improve component quality and productivity. Spindle speed affects surface roughness and cutting force for both MSS grades. Depth of cut affects both MSS classes' cutting temperature. Depth of cut affects both MSS classes' cutting temperature. Surface roughness and cutting force are higher in MSS AISI 420 because to its higher chromium and carbon composition. ANOVA shows that spindle speed, followed by feed and cutting depth, most affects Ra of both grades. According

to ANOVA results for both grades, spindle speed, feed, and depth of cut affected F_c the most. ANOVA findings for both grades reveal that feed, spindle speed, and depth of cut all affect temperature [15]. The mechanism that governs the milling process is depicted in Fig. 1.

From the literature, it was found that many researchers have already worked on CNC milling machining using various materials such as steels and composites. But for Cu-based SMAs till today, no work was carried out and reports are not available on milling studies of CAM SMAs [16]. Hence, new trail is carried out to evaluate the factors and their effect on the output responses, such as MRR and surface roughness, using the Taguchi method. The most popular optimisation approaches are Taguchi method, full factorial designs, and others. The Taguchi strategy, however, is one of the best techniques for optimisation as it needs the fewest tests while taking into account all relevant sets of input variables that can possibly have a big impact on the result. The goal of the current effort is to assess the output parameters with different input elements, such as depth of cut, feed, and spindle speed in order to maximise MRR and minimise Ra and provide an alloy surface finish of a higher grade.

Experimental Details

Materials and Method

From the literature, the alloy chosen is ductile in nature because of the presence of manganese in the Cu-Al binary alloy. In this experiment study, pure Cu, Al, and Mn of weight 200 g by varying the percentage of Al (10–13wt.%) and Mn (0–7.5wt.%) and rest being copper have been added and prepared alloy using induction melting process. Figure 2 shows the prepared seven samples of CAM SMAs for CNC Milling process. In this investigation, the as-cast samples of dimension 100X50X4mm (LXWXT) are homogenised at 900 °C for 45mints to 1 h to remove the agglomeration in the prepared alloy and to enhance uniformity in the composition.

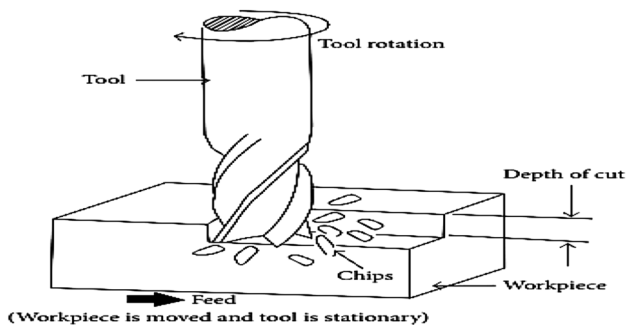


Fig. 1 CNC milling operation [16]



Fig. 2 Step quenched CAM SMA samples for CNC end milling machining

Later on the samples are betaized for 900 °C for 1 h and step quenched in hot water and cold water to relieve the internal stress present in the alloy and also the alloy is converted from austenite to martensite phase to obtain martensite structure.

Finally, the shape memory alloy is subjected to CNC end milling operation. Following the stage quenching procedure, Fig. 3 indicates that CAM SMA sample-7 has quenched cracks formation throughout its surface. As a result, alloy 7 exhibited poor machinability due to brittleness of the alloy; hence, this alloy is not suitable for CNC end milling operation and machining has been carried out for remaining six samples.

Chemical Compositions of CAM SMAs

The compositions chosen based on wt.%. The chemical compositions obtained after the sample preparation using optical spectrophotometer. Table 1 shows CAM SMA compositions.

Experimental Details

The current work was mostly completed using a CNC three-axis end milling machine. Based on a review of the literature, carbide was chosen as the material for cutting tools. A flat-end mill cutter with a 6 mm diameter has been

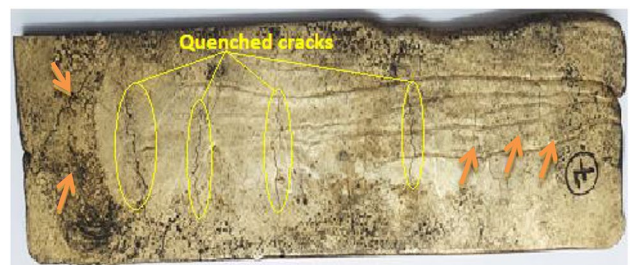


Fig. 3 Brittle CAM-7 SMA sample

Table 1 Compositions of CAM SMAs based on wt.%

Alloy ID	Cu	Al	Mn
<i>(Set-1-aluminium-constant)</i>			
CAM-1	88.5	10	1.5
CAM-2	86.5	10	3.5
CAM-3	84.5	10	5.5
CAM-4	82.5	10	7.5
<i>(Set-2-manganese-constant)</i>			
CAM-5	87.5	11	1.5
CAM-6	86.5	12	1.5
CAM-7	85.5	13	1.5

Table 2 Process parameters and their ranges

Process parameters	Level-1	Level-2	Level-3
Spindle speed (RPM)	400	800	1200
Feed rate (mm/min)	100	200	300
Depth of Cut (mm)	0.3	0.4	0.5



Fig. 4 Three axis vertical end milling machine



Fig. 5 Carbide flat-end mill cutter

chosen as the cutting tool. A CNC end milling machine was used in this particular experiment (Fig. 4). Figure 5 depicts the usage of a flat-type milling cutter as a cutting tool during a milling process. End milling was done on the workpiece material while it was dry utilising nine

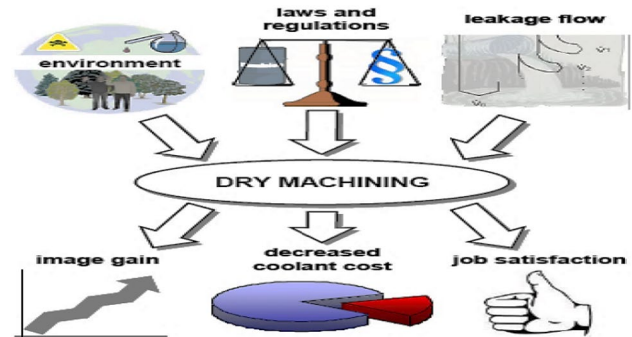


Fig. 6 Advantage of dry machining [24]

trials (i.e. a L9 orthogonal array) and adjusting the various parameters, as given in Table 2.

Machining Conditions

Cutting fluids harm the environment, economy, and health. Dry cutting, which fully forgoes the use of cutting fluids, is the greatest way to eradicate their effects. In addition to dry machining, there are also various machining conditions that can be utilised, such as wet machining, minimum quantity of lubricant (M.Q.L) machining, flooded machining, and cryogenic cooling. This type of machining uses no coolant, oil, or metal cutting fluid. It is mostly used in milling operations, not it is suggested for drilling operations. The use of cutting fluids in cutting operations causes significant economic, environmental, and health issues. Dry cutting, which fully forgoes the use of cutting fluids, is the greatest way to eradicate their effects which also lowers machining costs, environmental risks, and increase productivity [17–22]. However, this is not suitable for all machining operations and materials, and in some instances, dry cutting exhibits benefits including reduced thermal shock and extended tool life [23–27]. Dry machining does not need coolants. Consequently, the working atmosphere is more comfortable and clean, which eliminates the possibility of slippage when cutting [28–35]. Hence for the present investigation, a dry machining cutting condition is employed. Without the use of any cutting fluid, the machining process was carried out at 28 °C room temperature. Figure 6 shows the benefit in choosing dry condition for the present investigation as per the previous literature.

Results and Discussions

CAM SMA Samples after Milling Process

Figure 7 shows the CAM SMA samples obtained milling profile on the surface after undergoing CNC end milling operation. The samples are subjected to study the surface harshness using Mitutoyo surface roughness tester. Table 3 shows the milling data obtained based on Taguchi design and conducted the experiments using L9 orthogonal array. However, CNC milling was also carried out for all the seven samples of CAM SMAs. This combination of SMA was chosen because the addition of manganese concentration provides required ductility for the SMA [36–42]. For CAM-7 SMA, machining was unable to carry out due to the brittleness of the alloy taken place after step quenching process, because their parent phase has L21 structure due to the decrease in the degree of order [43–48]. A surface tester (Mitutoyo) was used to measure the texture that resulted from the machining process. For the analysis, the average roughness value (Ra) is taken into account. Figure 9 indicates the samples of CAM SMAs after milling operation.

The formulae used for evaluating MRR are as follows,



Fig. 7 Cu-Al-Mn SMA alloy samples after milling operation

$$MRR \text{ (gms/min)} = w_x d_x f_x \rho \tag{1}$$

where w —width of cut in mm, d —depth of cut, mm, f —feed rate in mm/min, and ρ —density of material in gm/cc.

S/N Plots for MRR and Ra

Figures 8 and 9 indicate the S/N curve for MRR and Ra. To determine MRR, “larger is better” method was chosen and “smaller is better”, for Ra. Figure 10 shows that the MRR was observed to be decreasing as spindle speed rose. Higher cut depths allow for the achievement of the maximum MRR [10]. According to the graph, MRR rises with rising feed rate and cutting depth, respectively. From Fig. 10, it was observed that an increase in feed rate and spindle speed tends to increase Ra value but decreases with an increase in feed rate. The MRR response data are shown in Table 4. Consequently, it was discovered that the feed rate is the

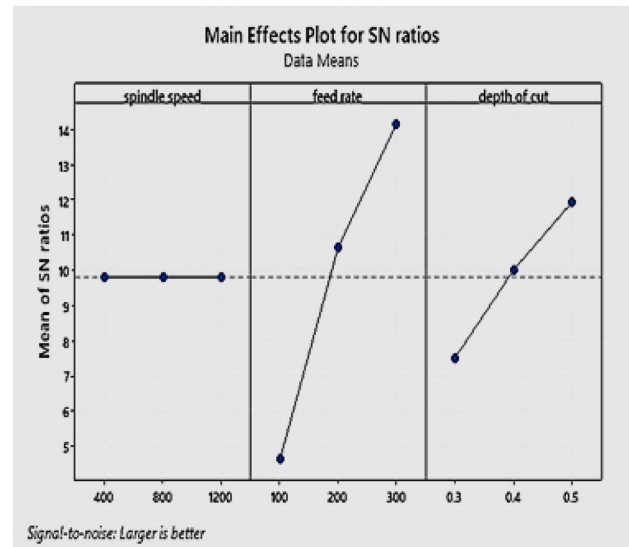


Fig. 8 S.N curve for MRR

Table 3 CNC end milling data of CAM SMAs for MRR

Sl. no	Spindle speed (rpm)	Feed (mm/rev)	Depth of cut (mm)	MRR (gms/min)	S/N Ratio	Ra (μm)	S/N ratio
1	400	100	0.3	1.305	2.3122	0.852	1.39121
2	400	200	0.4	3.480	10.8316	1.100	-0.827854
3	400	300	0.5	6.525	16.2916	1.243	-1.88942
4	800	100	0.4	1.740	4.8110	0.625	4.08240
5	800	200	0.5	4.350	12.7698	0.821	1.71314
6	800	300	0.3	3.915	11.8546	0.772	2.24765
7	1200	100	0.5	2.175	6.7492	0.426	7.41181
8	1200	200	0.3	2.610	8.3328	0.711	2.96261
9	1200	300	0.4	5.220	14.3534	0.598	4.46598

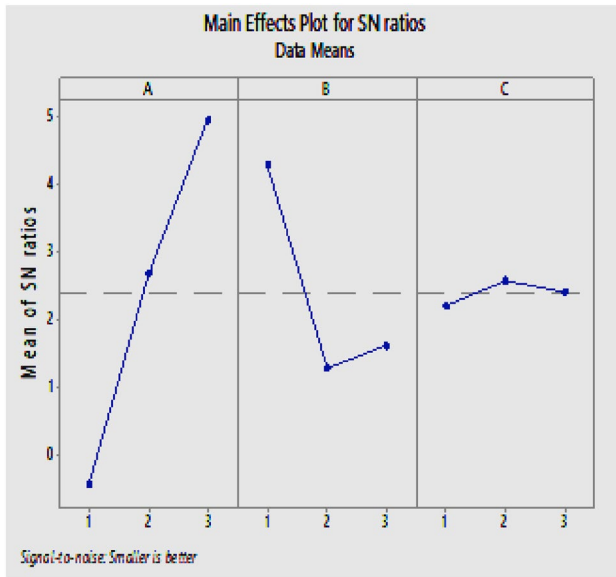


Fig. 9 S/N curve for Ra

primary characteristic that displayed rank-1. Because from the investigation, the feed rate is affecting more on MRR followed by depth of cut (rank-2) and spindle speed (rank-3). To evaluate MRR, larger the method was followed and for Ra the method followed is smaller the better. Table 5 shows that the spindle speed is ranked first, with depth of cut and feed rate coming in at positions two and three, respectively, as the key factors influencing Ra.

ANOVA for MRR and Ra

From Tables 6 and 7, it was observed that the %contribution is more for feed rate (77.42%) followed by cutting depth (19.35%) and spindle speed (1.21%) for MRR but for Ra, the % contribution is more for spindle speed (69.78%) followed by feed rate (16.50%) and depth of cut (0.79%), respectively. The probability value for feed rate is almost zero, followed by depth of cut (0.001) and spindle speed ($P > 0.144$) for MRR. The function is deemed to be insignificant if the values surpass 0.10. As a result, there is a 0.01 per cent chance that noise will have little effect. Similarly, it was noticed that the P value is less for spindle speed ($P < 0.003$) followed by feed rate ($p < 0.053$) and depth of cut ($P < 0.605$), respectively, for Ra. In case of MRR, feed rate and depth of cut are the two main important factors responsible for affecting the output response. Here, spindle speed was found as insignificant parameters because it is not affecting on output characteristic (i.e. Ra). In case of Ra, both feed rate and spindle speed are the main significant parameters affecting the Ra of Cu-Al-Mn SMAs. But this parameter (depth of cut) is showing least effect on Ra. However, it was considered as the insignificant parameter for Ra.

Surface Morphology of Milled Profile of CAM SMAs

Both MRR and Ra are highly sensitive to the machining conditions, which can be altered by adjusting factors including feed rate, depth of cut, and spindle speed. SEM analysis was investigated for the samples machined under CNC Milling operation. Figure 10 represents the difference between up milling and down milling under CNC end milling process. The burr size can vary as a result of this type of milling procedure. It was observed that compared to down milling, the height of the burr obtained during the up-milling operation is short. The up-milling procedure is followed to produce burrs with decreased height and thickness. The height of the burr during the down-milling process is higher than up-milling process, the burr thickness must be greater. In such constraint, the burr thickness in down milling is less. The volume of the material should remain the same during the deformation process, as recommended by the principles of plastic deformation. Therefore, in order to satisfy the criterion of a constant burr volume, the burr thickness must be increased if, during the up-milling process, the burr height is lower than it was during the down-milling process. Under these circumstances, the burr thickness achieved through down milling is lower [49–55].

Figure 10a shows the milling profile of CAM-4 SMAs. Here the tool rotation direction up-milling side and down-milling side, feed applied direction can be observed and ring type of profile formed at the milled slot of the alloy. From Fig. 10b, milling burrs, individual milling grooves, flank profile of milling groove, bottom of milling grooves after each trail of milling operation during dry machining condition were observed. The slot side is the side portion which is not machined and slot base is the base of the milled profile [56–60].

SEM pictures of the machined surfaces taken in dry conditions, as shown in Fig. 10c, can be used to identify various surface flaws. It was clear that the ring-shaped grooves and smears spread over the machined surface throughout the dry machining process. It consists of smooth and rough surfaces during the operation, formation of voids and chips can also be observed at spindle speed—1200RPM, feed—100 mm/rev, and depth of cut—0.5 mm, respectively.

First, because of the slower feed rate of 100 mm/rev, no feed marks are visible. The second observation is that there are no waves or ridges of any type on the surface. This is because there is less of a cutting force, which results in less plastic deformation and, as a result, a smoother surface. It is possible that the vibrations produced are responsible for the creation of waves on the surface, but it might also be the result of tool wear, which led the material to shift from a surface that was machined by one flute of the tool to a surface machined by the second flute of the tool, respectively [61–65]. Regardless of the reason, the waves can be seen as

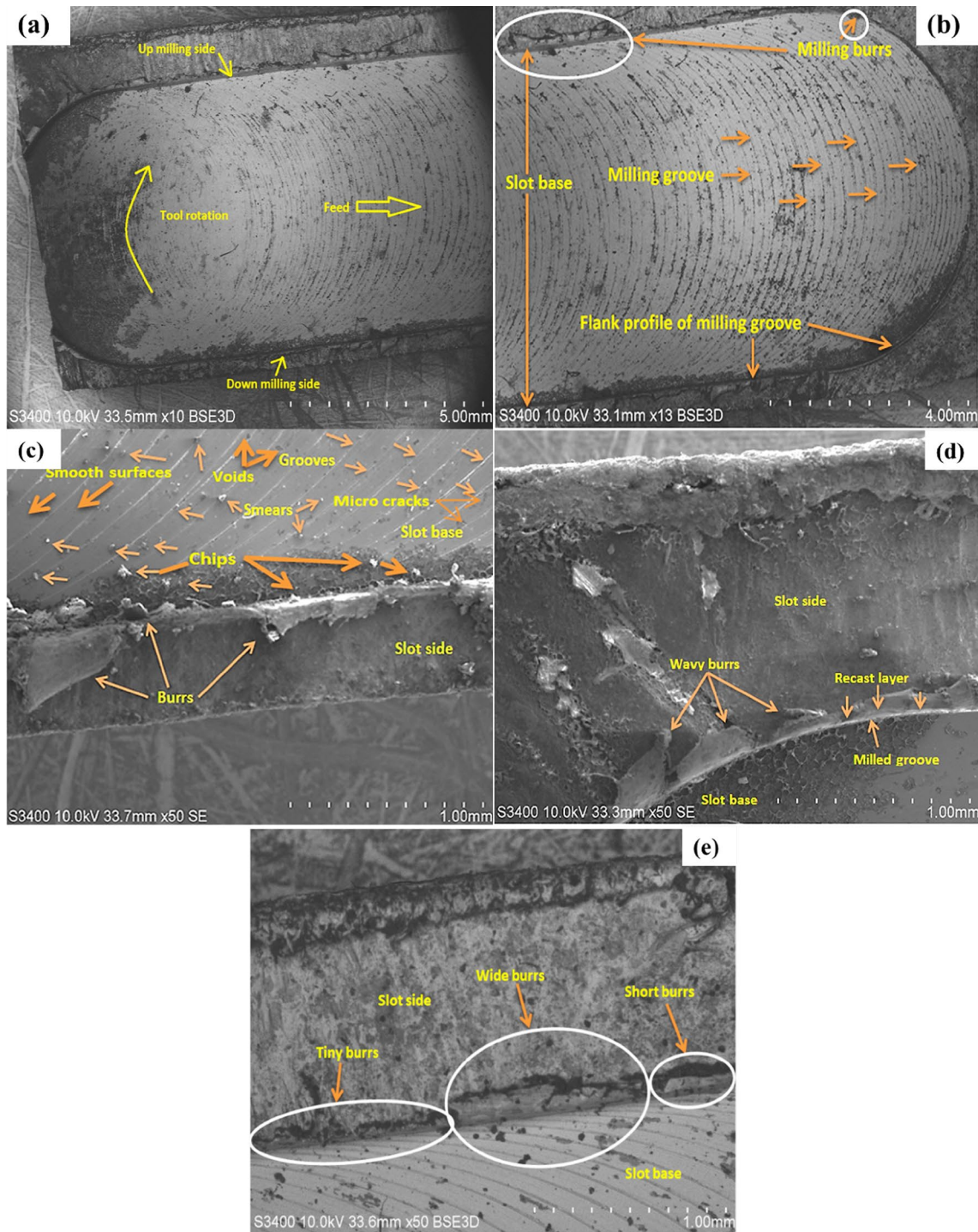


Fig. 10 a–e CNC milling profile of CAM-4 SMA under dry condition

an undesirable feature. In a similar fashion, there were found to be some micro-cracks observed over the machined surface. Due to insufficient material removal from the surface, micro-cracks developed on the surface [66, 67].

Figure 10d shows the uneven sized burrs with varying height and thickness at the milled groove end. At the

sidewalls of the channel, recast layer development was also seen. Because of maximum amount of heat generated between the rotating tool and workpiece interface melts the material rapidly responsible for the structure of cast layer. Figure 10e indicates initially when machining starts with rotating tool movement leads to the structure of tiny burrs,

Table 4 Response table for MRR

Larger is better			
Levels	Spindle speed	Feed rate	Depth of cut
1	9.812	4.624	7.500
2	9.812	10.645	9.999
3	9.812	14.167	11.937
Delta	0.000	9.542	4.437
Rank	3	1	2

Table 5 Response data for Ra

Smaller is better			
Levels	Spindle speed	Feed rate	Depth of cut
1	-0.442	4.2951	2.2005
2	2.6811	1.2826	2.5735
3	4.9468	1.6081	2.4118
Delta	5.3888	3.0125	0.373
Rank	1	2	3

further movement of tool results in wider burrs of varied thickness and height, and finally, the forms short burrs with small thickness and height in each trail can be observed, respectively [68–71].

Conclusions

Below is a summary of the findings from the experimental research on Cu-Al-Mn SMAs, along with any inferences that may be made.

- Based on experimental findings of MRR and Ra, which are mostly connected to speed and feed rate followed by depth of cut, the approach employed in this work focuses on analysis of CNC milling parameters to achieve optimal values of the output parameters. The machining parameters have been optimised using Taguchi design.
- By exhibiting relative contributions of 77.42%, 19.35%, and 1.21% in the ANOVA findings, spindle speed, depth of cut, and feed rate were identified as the parameters influencing MRR. When compared to the other two factors (such as depth of cut spindle speed), it was discovered that the feed rate’s percentage contribution has a greater impact on MRR. The rank values demonstrate that the influence of feed rate on MRR is greater. Therefore, extending the depth of cut will result in the greatest amount of material (MRR).
- According to the analysis, the two primary factors most significantly determine surface roughness (Ra) relative to spindle speed, depth of cut, and feed rate. The ideal MRR and Ra values are achieved at the first level spindle speed (400 rpm), third level depth of cut (0.5 mm), and third level feed rate (300 mm/min). Ra at spindle’s third level (1200 RPM), first level feed rate (100 mm/Rev), and third level cut depth (0.5 mm). The smallest amount of roughness needed to provide a decent surface finish can be obtained by lowering spindle speed.
- The profile was created via a CNC end milling operation, as seen by SEM pictures. The surface morphology of the machined produced changes according on the input parameter values used, as seen by images taken using a SEM. It has been discovered that the rotation and movement of the tool during the end milling process causes the production of wavy burrs, short burrs, long burrs, and rings by rings kinds of burrs.

Table 6 ANOVA for MRR

Source	DF	Seq SS	Adj SS	Adj MS	F value	P value	% contribution
Spindle speed	1	0.2838	0.2838	0.2838	3.00	0.144	1.21%
Feed rate	1	18.1656	18.1656	18.1656	192.00	0.000	77.42%
Depth of cut	1	4.5414	4.5414	4.5414	48.00	0.001	19.35%
Error	5	0.4731	0.4731	0.0946			2.02%
Total	8	23.4639					100.00%

Table 7 ANOVA for Ra

Source	DF	Seq SS	Adj SS	Adj MS	F value	P value	% contribution
Spindle speed	1	0.355267	0.355267	0.355267	26.99	0.003	69.78%
Feed rate	1	0.084017	0.084017	0.084017	6.68	0.053	16.50%
Depth of cut	1	0.004004	0.004004	0.004004	0.3	0.605	0.79%
Error	5	0.065816	0.065816	0.013163			12.93%
Total	8	0.509104					100%

- From the entire analysis, it can be inferred that the brittle samples of CAM SMAs are not appropriate for the CNC end milling operation, which may be used to provide a higher surface finish for ductile SMAs. Brittle alloys are created as a result of the Cu-matrix's increased Al content and decreased Mn concentration. As a result, the CAM-7 alloy (Cu—85.5%, Al—13%, and Mn—1.5%) displayed hard and brittle behaviour, and following milling, powdered sort rather than chips were produced. This specific composition has been shown to be poorly machinable and unsuitable for any machining operation.
- This end milling process is suitable where the smart materials component manufacturing takes place. For industrial sectors where batch production of component manufacturing takes place, it is primarily low cost and simple to manufacture with higher precision, which will be unquestionably advantageous both economically and commercially.

Acknowledgements The research was carried out at Siddaganga Institute of Technology, Tumakuru, with the support of a research assistantship and excellent research facilities. Special thanks go out to Ramaiah University of Applied Science College, Bangalore, for funding the CNC milling facility.

Funding This work did not receive any financial support.

Data availability Not applicable.

Declarations

Conflict of interest A conflict of interest is not present, according to the authors.

References

1. A. Mielczarek, W. Riehemann, S. Vogelgesang, B. Tonn, Mechanical and fatigue properties of Cu-Al-Mn shape memory alloys with influence of mechanical cycling on amplitude dependence of internal friction at room temperature. *Solid State Phenom.* **137**, 145–154 (2008)
2. R. Suresh Kumar, S. Senthil Kumar, K. Murugan, B. Guruprasad, S. Manavalla, S. Madhu, Optimization of CNC end milling process parameters of low-carbon mold steel using response surface methodology and grey relational analysis. *Adv. Mater. Sci. Eng.* **2021**, 11 (2021). <https://doi.org/10.1155/2021/4005728>
3. Malay, K. Gupta, J. Gangwar, H.N. Khan, N.P. Sharma, A. Mandal, S. Kumar, R. Garg, Optimization of process parameters of CNC milling. *Int. J. Adv. Res. Innov.* **3**(4), 59–63 (2016)
4. B.H.C. Kalyan, V.V. Reddy, Optimization of milling parameters for HDPE plastic using genetic algorithm. *J. Eng. Sci.* **10**(12), 9–14 (2019)
5. B. Fabien, P. Vijayakumar, Process parametric optimization of CNC vertical milling machine using ANOVA method in EN24. *J. Res. Appl. Sci. Eng. Technol.* (2022). <https://doi.org/10.22214/ijraset.2022.43008>
6. S.B. Sahare, S.P. Untawale, S.S. Chaudhari, R.L. Shrivastav, Experimental investigation of end milling operation on Al2024. *Mater. Today Proc.* **4**(2), 1357–1365 (2017)
7. R. Sreenivasulu, S.H. Hussain, R.V. RamaKrishna, R.V. Dasari, P. Suresh, Experimental studies on effect of machining parameters on burr height during end milling of Inconel 718 super alloys. *Eng. Technol. J.* **3**(03), 389–393 (2018)
8. S.K. Mishra, Study of performance of milling machine for optimum surface roughness study of performance of milling machine for optimum surface roughness. *Res. J. Eng. Sci.* **6**(9), 32–35 (2017)
9. A. Gupta, P.K. Soni, C.M. Krishna, Modeling and analysis of CNC milling process parameters on Al3030 based composite. In: *IOP Conference Series: Material Science Engineering*, vol. 346, p. 012073 (2018)
10. M.L.M. Ramanujam, R.K.J. VenkatesanJerald, Optimization of machining parameters for end milling of Inconel 718 super alloy using Taguchi based grey relational analysis. *Procedia Eng.* **64**, 1276–1282 (2013)
11. L. Prasetyo, M. Tauviqirrahman, Rusnaldy, A study of chip formation feedrates of various steels in low-speed milling process. In: *IOP Conference Series: Materials Science and Engineering*, vol. 202, p. 012097
12. B.C. Routara, A. Bandyopadhyay, P. Sahoo, Roughness modeling and optimization in CNC end milling using response surface method: effect of workpiece material variation. *Int. J. Adv. Manuf. Technol.* **40**, 1166–1180 (2009)
13. S.B. Raja, N. Baskar, Application of particle swarm optimization technique for achieving desired milled surface roughness in minimum machining time. *Expert Syst. Appl.* **39**, 5982–5989 (2012)
14. P.H. Syeddu, V. Jayakumar, G. Bharathiraja, Experimental investigation on surface roughness in CNC end milling process by uncoated and TiAlN coated carbide end mill under dry conditions. *Mater. Today Proc.* (2019)
15. P. George, D.P. Selvaraj, Optimization of cutting parameters of martensitic stainless steel grades AISI 410 and AISI 420 during CNC dry milling. *J. Eng. Sci. Technol.* **16**(6), 4369–4382 (2021)
16. M. Nurhaniza, M.K.A.M. Ariffin, F. Mustapha, B.T.H.T. Baharudin, Analyzing the effect of machining parameters setting to the surface roughness during end milling of CFRP-aluminium composite laminates. *Int. J. Manuf. Eng.* **2016**, 4680380 (2016). <https://doi.org/10.1155/2016/4680380>
17. S. Akula, S.N. Nayak, G. Bolar, V. Managuli, Comparison of conventional drilling and helical milling for hole making in Ti6Al4V titanium alloy under sustainable dry condition. *Manuf. Rev.* **8**, 12 (2021). <https://doi.org/10.1051/mfreview/2021010>
18. A. Shokrani, V. Dhokia, S.T. Newman, International journal of machine tools & manufacture environmentally conscious machining of difficult-to-machine materials with regard to cutting fluids. *Int. J. Mach. Tools Manuf.* **57**, 83–101 (2012)
19. C. Bandapalli, K.K. Singh, B.M. Sutaria, D.V. Bhatt, Experimental investigation of top burr formation in high-speed micro-end milling of titanium alloy. *Mach. Sci. Technol.* **22**(6), 989–1011 (2018). <https://doi.org/10.1080/10910344.2018.1449213>
20. M.N. Trimbakwade, M.T. Shete, Optimization of CNC face milling process parameters for Inconel 718 by using Taguchi method—a review. *Int. Res. J. Eng. Technol. (IRJET)* **04**(04), 806–810 (2017)
21. J.H. Kim, E.J. Kim, C.M. Lee, A study on the heat affected zone and machining characteristics of difficult-to-cut materials in laser and induction assisted machining. *J. Manuf. Process.* **57**, 499–508 (2020)
22. Z. Pan, Y. Feng, T.-P. Hung, Y.-C. Jiang, F.-C. Hsu, Wu. Lung-Tien et al., Heat affected zone in the laser-assisted milling of Inconel 718. *J. Manuf. Process.* **30**, 141–147 (2017)

23. N. Praveen, U.S. Mallik, A.G. Shivasiddaramaiah, G.N. Reddy, A study on material removal rate of Cu-Al-Mn shape memory alloys in WEDM. *Mater. Today Proc.* **46**, 2–6 (2021)
24. N. Praveen, U.S. Mallik, L. Shivaramu, A.G. Shivasiddaramaiah, S.R. Suresh, S. Prashantha, Synthesis and evaluation of machining characteristics of Cu-Al-Mn ternary shape memory alloys using CNC wire electric discharge machining. In: *AIP Conference Proceedings*, vol. 2247
25. V. Sampath, U.S. Mallik, Influence of minor additions of boron and zirconium on shape memory properties and grain refinement of a Cu-Al-Mn shape memory alloy. *ESOMAT* **2009**, 05028 (2009). <https://doi.org/10.1051/esomat/200905028>
26. T. Batra, P.S. Rao, Analyzing the effect of different process parameters on tool wear, chip formation and surface integrity during CNC milling of hastelloy C-276. *Int. Res. J. Eng. Technol.* **2631–2634** (2017)
27. M. Yasir, T.L. Ginta, B. Ariwahjoedi, A.U. Alkali, M. Danish, Effect of cutting speed and feed rate on surface roughness of AISI 316L Ss using end-milling. *ARPN J. Eng. Appl. Sci.* **11**(4), 2496–2500 (2016)
28. C. Durga Prasad, S. Joladarashi, M.R. Ramesh, M.S. Srinath, Microstructure and tribological resistance of flame sprayed CoMoCrSi/WC-CrC-Ni and CoMoCrSi/WC-12Co composite coatings remelted by microwave hybrid heating. *J. Bio Tribo-Corros.* **6**, 124 (2020). <https://doi.org/10.1007/s40735-020-00421-3>
29. C. Durga Prasad, S. Joladarashi, M.R. Ramesh, Comparative investigation of HVOF and flame sprayed CoMoCrSi coating. *Am. Inst. Phys.* **2247**, 050004 (2020). <https://doi.org/10.1063/5.0003883>
30. M. Arunadevi, M. Rani, R. Sibinraj, M.K. Chandru, C. Durga Prasad, Comparison of k-nearest neighbor & artificial neural network prediction in the mechanical properties of aluminum alloys. *Mater. Today Proc.* (2023). <https://doi.org/10.1016/j.matpr.2023.09.111>
31. C. Durga Prasad, A. Jerri, M.R. Ramesh, Characterization and sliding wear behavior of iron based metallic coating deposited by HVOF process on low carbon steel substrate. *J. Bio Tribo-Corros.* **6**, 69 (2020). <https://doi.org/10.1007/s40735-020-00366-7>
32. M.A. Kattimani, P.R. Venkatesh, H. Masum, M.M. Math, V.N. Bahadurdesai, S. Mustafkhadri, C. Durga Prasad, H. Vasudev, Design and numerical analysis of tensile deformation and fracture properties of induction hardened inconel 718 superalloy for gas turbine applications. *Int. J. Interact. Design Manuf. (IJIDeM)* (2023). <https://doi.org/10.1007/s12008-023-01452-z>
33. C. Durga Prasad, S. Joladarashi, M.R. Ramesh, M.S. Srinath, B.H. Channabasappa, Comparison of high temperature wear behavior of microwave assisted HVOF sprayed CoMoCrSi-WC-CrC-Ni/WC-12Co composite coatings. *SILICON* **12**, 3027–3045 (2020). <https://doi.org/10.1007/s12633-020-00398-1>
34. C. Manjunatha, T.N. Sreenivasa, P. Sanjay et al., Optimization of friction stir welding parameters to enhance weld nugget hardness in AA6061-B₄C composite material. *J. Inst. Eng. India Ser. D* (2023). <https://doi.org/10.1007/s40033-023-00562-y>
35. C. Durga Prasad, S. Joladarashi, M.R. Ramesh, M.S. Srinath, B.H. Channabasappa, Effect of microwave heating on microstructure and elevated temperature adhesive wear behavior of HVOF deposited CoMoCrSi-Cr₃C₂ composite coating. *Surf. Coat. Technol.* **374**, 291–304 (2019). <https://doi.org/10.1016/j.surfcoat.2019.05.056>
36. C. Durga Prasad, S. Joladarashi, M.R. Ramesh, M.S. Srinath, B.H. Channabasappa, Development and sliding wear behavior of Co-Mo-Cr-Si cladding through microwave heating. *SILICON* **11**, 2975–2986 (2019). <https://doi.org/10.1007/s12633-019-0084-5>
37. C. Durga Prasad, S. Joladarashi, M.R. Ramesh, M.S. Srinath, B.H. Channabasappa, Microstructure and tribological behavior of flame sprayed and microwave fused CoMoCrSi/CoMoCrSi-Cr₃C₂ coatings. *Mater. Res. Express* **6**, 026512 (2019). <https://doi.org/10.1088/2053-1591/aeabd9>
38. H. Sharanabasava, M. Raviprakash, C. Durga Prasad, M.R. Ramesh, M.V. Phanibhushana, H. Vasudev, S. Kumar, Microstructure, mechanical and wear properties of SiC and Mo reinforced NiCr microwave cladding. *Adv. Mater. Process. Technol.* (2023). <https://doi.org/10.1080/2374068X.2023.2257937>
39. C. Durga Prasad, S. Kollur, M. Nusrathulla, G. Satheesh Babu, M.B. Hanamantraygouda, B.N. Prashanth, N. Nagabhushana, Characterisation and wear behaviour of SiC reinforced FeNiCrMo composite coating by HVOF process. *Trans. IMF* (2023). <https://doi.org/10.1080/00202967.2023.2246259>
40. M.A. Kattimani, P.R. Venkatesh, L.J. Kirthan, M.M. Math, A.C. Prapul Chandra, R. Hegde, C. Durga Prasad, M. Gupta, S. Kumar, Design and optimization of fatigue life studies on induction hardened IN718 alloy for gas turbine applications. *Adv. Mater. Process. Technol.* (2023). <https://doi.org/10.1080/2374068X.2023.2256121>
41. A.K.R. Tavadi, N. Nagabhushana, V.N. Vivek Bhandarkar, T. Jagadeesha, M.R. Kerur, S. Rudresha, C. Durga Prasad, A. Rajesh Kannan, D.G. Mohan, Investigation on mechanical and sliding wear behaviour of pongamia-oil-cake/basalt fibre reinforced epoxy hybrid composites. *Arab. J. Sci. Eng.* (2023). <https://doi.org/10.1007/s13369-023-08207-8>
42. A. Rajesh Kannan, C. Durga Prasad, V. Rajkumar, N. Siva Shanmugam, V. Rajkumar, W. Lee, J. Yoon, Hot oxidation and corrosion behaviour of boiler steel fabricated by wire arc additive manufacturing. *Mater. Charact.* **203**, 113113 (2023). <https://doi.org/10.1016/j.matchar.2023.113113>
43. G.S. Kulkarni, N.G. Siddeshkumar, C. Durga Prasad, L. Shankar, R. Suresh, Drilling of GFRP with liquid silicon rubber reinforced with fine aluminium powder on hole surface quality and tool wear using DOE. *J. Bio Tribo-Corros.* **9**, 53 (2023). <https://doi.org/10.1007/s40735-023-00771-8>
44. S.D. Kulkarni, M.U. Chandrasekhar, K.V. Manjunath, C. Durga Prasad, H. Vasudev, Design and optimization of polyvinyl-nitrile rubber for tensile strength analysis. *Int. J. Interact. Design Manuf. (IJIDeM)* (2023). <https://doi.org/10.1007/s12008-023-01405-6>
45. M.M. Math, K.V.S. Rajeswara Rao, A.C. Prapul Chandra, M.N. Vijayakumar, B. Nandini, C. Durga Prasad, H. Vasudev, Design and modeling using finite element analysis for the sitting posture of computer users based on ergonomic perspective. *Int. J. Interact. Design Manuf. (IJIDeM)* (2023). <https://doi.org/10.1007/s12008-023-01383-9>
46. G. Madhu Sudana Reddy, C. Durga Prasad, S. Kollur, A. Lakshminathan, R. Suresh, C.R. Aprameya, Investigation of high-temperature erosion behavior of NiCrAlY/TiO₂ plasma coatings on titanium substrate. *JOM J. Min. Metals Mater. Soc. (TMS)* (2023). <https://doi.org/10.1007/s11837-023-05894-4>
47. P. Nagabhushana, S. Ramprasad, C. Durga Prasad, H. Vasudev, C. Prakash, Numerical investigation on heat transfer of a nano-fluid saturated vertical composite porous channel packed between two fluid layers. *Int. J. Interact. Design Manuf. (IJIDeM)* (2023). <https://doi.org/10.1007/s12008-023-01379-5>
48. N. Praveen, U.S. Mallik, A.G. Shivasiddaramaiah, R. Suresh, C. Durga Prasad, L. Shivaramu, Synthesis and wire EDM characteristics of Cu-Al-Mn ternary shape memory alloys using Taguchi method. *J. Inst. Eng. (India) Series D* (2023). <https://doi.org/10.1007/s40033-023-00501-x>
49. G. Anjaneya, S. Sunil, S. Kakkeri, M.M. Math, M.N. Vaibhav, C. Solaimuthu, C. Durga Prasad, H. Vasudev, Numerical simulation of microchannel heat exchanger using CFD. *Int. J. Interact. Design Manuf. (IJIDeM)* (2023). <https://doi.org/10.1007/s12008-023-01376-8>
50. M. Poojari, H. Hanumanthappa, C. Durga Prasad, H.M. Jathanna, A.R. Ksheerasagar, P. Shetty, B.K. Shanmugam, H. Vasudev,

- Computational modelling for the manufacturing of solar-powered multifunctional agricultural robot. *Int. J. Interact. Design Manuf. (IJIDeM)* (2023). <https://doi.org/10.1007/s12008-023-01291-y>
51. C.J. Manjunatha, C. Durga Prasad, H. Hanumanthappa, A. Rajesh Kannan, G.M. Dhanesh, B.K. Shanmugam, C. Venkategowda, Influence of microstructural characteristics on wear and corrosion behaviour of Si₃N₄ reinforced Al2219 composites. *Adv. Mater. Sci. Eng.* **2023**, 1120569 (2023). <https://doi.org/10.1155/2023/1120569>
 52. H. Sharanabasva, C. Durga Prasad, M.R. Ramesh, Characterization and wear behavior of NiCrMoSi microwave cladding. *J. Mater. Eng. Perform.* (2023). <https://doi.org/10.1007/s11665-023-07998-z>
 53. H.S. Nithin, K.M. Nishchitha, D.G. Pradeep, C. Durga Prasad, M. Mathapati, Comparative analysis of CoCrAlY coatings at high temperature oxidation behavior using different reinforcement composition profiles. *Weld. World* **67**, 585–592 (2023). <https://doi.org/10.1007/s40194-022-01405-2>
 54. D.C. Naveen, K. Naresh, B.S. Keerthi Gowda, G. Madhu Sudana Reddy, C.D. Prasad, R. Shanmugam, Effects of polypropylene waste addition as coarse aggregates in concrete: experimental characterization and statistical analysis. *Adv. Mater. Sci. Eng.* **2022**, 11 (2022). <https://doi.org/10.1155/2022/7886722>
 55. H. Sharanabasva, C. Durga Prasad, M.R. Ramesh, Effect of Mo and SiC reinforced NiCr microwave cladding on microstructure, mechanical and wear properties. *J. Inst. Eng. (India) Series D* (2023). <https://doi.org/10.1007/s40033-022-00445-8>
 56. G. Madhusudana Reddy, C. Durga Prasad, P. Patil, N. Kakur, M.R. Ramesh, Elevated temperature erosion performance of plasma sprayed NiCrAlY/TiO₂ coating on MDN 420 steel substrate. *Surf. Topogr. Metrol. Prop.* **10**, 025010 (2022). <https://doi.org/10.1088/2051-672X/ac6a6e>
 57. V. Gowda, H. Hanumanthappa, B.K. Shanmugam, C. Durga Prasad, T.N. Sreenivasa, M.S. Rajendra Kumar, High-temperature tribological studies on hot-forged Al6061–TiB₂ in situ composites. *J. Bio Tribo-Corros.* **8**, 101 (2022). <https://doi.org/10.1007/s40735-022-00699-5>
 58. G. Madhusudana Reddy, C. Durga Prasad, G. Shetty, M.R. Ramesh, T. Nageswara Rao, P. Patil, Investigation of thermally sprayed NiCrAlY/TiO₂ and NiCrAlY/Cr₂O₃/YSZ cermet composite coatings on titanium alloys. *Eng. Res. Express* **4**(2), 025049 (2022). <https://doi.org/10.1088/2631-8695/ac7946>
 59. T. Naik, M. Mathapati, C. Durga Prasad, H.S. Nithin, M.R. Ramesh, Effect of laser post-treatment on microstructural and sliding wear behavior of HVOF-sprayed NiCrC and NiCrSi coatings. *Surf. Rev. Lett.* **29**(01), 2250007 (2022). <https://doi.org/10.1142/S0218625X2250007X>
 60. G. Madhusudana Reddy, C. Durga Prasad, G. Shetty, M.R. Ramesh, T. Nageswara Rao, P. Patil, High-temperature oxidation behavior of plasma-sprayed NiCrAlY/TiO₂ and NiCrAlY/Cr₂O₃/YSZ coatings on titanium alloy. *Weld World* (2022). <https://doi.org/10.1007/s40194-022-01268-7>
 61. M. Mathapati, K. Amate, C. Durga Prasad, M.L. Jayavardhana, T. Hemanth Raju, A review on fly ash utilization. *Mater. Today Proc.* **50**, 1535–1540 (2022). <https://doi.org/10.1016/j.matpr.2021.09.106>
 62. G. Madhusudana Reddy, C. Durga Prasad, G. Shetty, M.R. Ramesh, T. Nageswara Rao, P. Patil, High temperature oxidation studies of plasma sprayed NiCrAlY/TiO₂ & NiCrAlY /Cr₂O₃/YSZ cermet composite coatings on MDN-420 special steel alloy. *Metall. Microstruct. Anal.* **10**, 642–651 (2021). <https://doi.org/10.1007/s13632-021-00784-0>
 63. R. Dinesh, S. Rohan Raykar, T.L. Rakesh, M.G. Prajwal, S.M. Lingappa, C. Durga Prasad, Feasibility study on MoCoCrSi/WC-Co cladding developed on austenitic stainless steel using microwave hybrid heating. *J. Mines Metals Fuels* **69**(12A), 260–264 (2021). <https://doi.org/10.18311/jmmf/2021/30113>
 64. C.D. Prasad, S. Lingappa, S. Joladarashi, M.R. Ramesh, B. Sachin, Characterization and sliding wear behavior of CoMoCrSi+ Flyash composite cladding processed by microwave irradiation. *Mater. Today Proc.* **46**, 2387–2391 (2021). <https://doi.org/10.1016/j.matpr.2021.01.156>
 65. G. Madhu, K.M. Mrityunjaya Swamy, D.A. Kumar, C. Durga Prasad, U. Harish, Evaluation of hot corrosion behavior of HVOF thermally sprayed Cr₃C₂-35NiCr coating on SS 304 boiler tube steel. *Am. Inst. Phys. cs* **2316**, 030014 (2021). <https://doi.org/10.1063/5.0038279>
 66. M. Reddy, C.D. Prasad, P. Patil, M.R. Ramesh, N. Rao, Hot corrosion behavior of plasma-sprayed NiCrAlY/TiO₂ and NiCrAlY/Cr₂O₃/YSZ cermets coatings on alloy steel. *Surf. Interfaces* **22**, 100810 (2021). <https://doi.org/10.1016/j.surf.2020.100810>
 67. K.G. Girisha, K.S. Rao, C.D. Prasad, Slurry erosion resistance of martensitic stainless steel with plasma sprayed Al₂O₃-40% TiO₂ coatings. *Mater. Today Proc.* **5**, 7388–7393 (2018). <https://doi.org/10.1016/j.matpr.2017.11.409>
 68. C. Durga Prasad, S. Joladarashi, M.R. Ramesh, M.S. Srinath, B.H. Channabasappa, Influence of microwave hybrid heating on the sliding wear behaviour of HVOF sprayed CoMoCrSi coating. *Mater. Res. Express* **5**, 086519 (2018). <https://doi.org/10.1088/2053-1591/aad44e>
 69. K.G. Girisha, R. Rakesh, C. Durga Prasad, K.V. Sreenivas Rao, Development of corrosion resistance coating for AISI 410 grade steel. *Appl. Mech. Mater.* **813–814**, 135–139 (2015). <https://doi.org/10.4028/www.scientific.net/AMM.813-814.135>
 70. C. Durga Prasad, S. Joladarashi, M.R. Ramesh, A. Sarkar, High temperature gradient cobalt based clad developed using microwave hybrid heating. *Am. Inst. Phys.* **1943**, 020111 (2018). <https://doi.org/10.1063/1.5029687>
 71. K.G. Girisha, C. Durga Prasad, K.C. Anil, K.V. Sreenivas Rao, Dry sliding wear behaviour of Al₂O₃ coatings for AISI 410 grade stainless steel. *Appl. Mech. Mater.* **766–767**, 585–589 (2015). <https://doi.org/10.4028/www.scientific.net/AMM.766-767.585>

Publisher's Note Springer Nature remains neutral with regard to jurisdictional claims in published maps and institutional affiliations.

Springer Nature or its licensor (e.g. a society or other partner) holds exclusive rights to this article under a publishing agreement with the author(s) or other rightsholder(s); author self-archiving of the accepted manuscript version of this article is solely governed by the terms of such publishing agreement and applicable law.